


Cite this: *RSC Adv.*, 2021, 11, 34898

# Fluorescent N-functionalized carbon nanodots from carboxymethylcellulose for sensing of high-valence metal ions and cell imaging†

Zhenzhen Liu,<sup>c</sup> Runsen Li,<sup>c</sup> Yan Li,<sup>c</sup> Jingpeng Zhou,<sup>d</sup> Yumei Gong,<sup>c</sup> <sup>c</sup> Haiqiang Shi,<sup>c</sup> Yanzhu Guo,<sup>c</sup> <sup>\*abcd</sup> Haiming Li,<sup>\*c</sup> Zhiwei Wang<sup>\*a</sup> and Fengshan Zhang<sup>d</sup>

A convenient and sensitive reversible-fluorescence sensing platform for accurate monitoring of high-valence metal ions is still very challenging. As a green kind of fluorescent carbon nanomaterials, carbon dots (CDs) have captured considerable attention because of the stable fluorescence property and low cost. Herein, we fabricated a type of nitrogen-functionalized carbon dots (N-CDs) from CMC as a fluorescent reversible sensing platform for detecting various high-valence metal ions. N-CDs with a mean size of 2.3 nm were obtained and possessed 22.9% quantum yields (QY). A label-free fluorescent probe for detection of high-valence metal ions ( $\text{Fe}^{3+}$ ,  $\text{Cr}^{6+}$ ,  $\text{Mn}^{7+}$ ) was established via the fluorescence quenching response. Among them, the detection limit (LOD) toward  $\text{Fe}^{3+}$  ions reached 0.8  $\mu\text{M}$ . We have explored the quenching mechanism of N-CDs to explain the valence state-related electron-transfer fluorescence quenching between high-valence metal ions and N-CDs. Moreover, the valence state-related fluorescence quenching phenomenon of N-CDs in aqueous solution could be effectively recovered by introducing a reducing agent ( $\text{Ti}^{3+}$ ). This "turn off-on" fluorescence recovery system of N-CDs could be applied in different applications covering the selective detection of environmental high-valence metal ions and cellular imaging.

Received 27th June 2021  
Accepted 20th October 2021

DOI: 10.1039/d1ra04972k

rsc.li/rsc-advances

## 1. Introduction

Heavy metal ions are potentially toxic metal elements that affect human physical health. Due to the growth of anthropic activity and rapid modern development, the presence of heavy metal ions ( $\text{Cr}^{6+}$  and  $\text{Mn}^{7+}$ ), which are released from heavy metal-using industrial plants in processes such as the tanning of leather, electroplating and pigment production, has undergone a sharp increase over a period of years. In addition,  $\text{Fe}^{3+}$  ions, as an important trace element in the human body, are involved in various biological reactions in the body, e.g., oxygen transport, energy conversion, enzyme catalysis and metabolism regulation.<sup>1</sup> The contents of such essential ions in the body must be maintained at an appropriate level, and any lack or excess of them can lead to human disease or biological toxicity.<sup>2</sup>

Therefore, it is a critical issue to dig out economical and accurate methods for selective detection of metal ions, aiming to alleviate environmental pollution and protect human health. To date, various techniques for detecting metal ions include but are not limited to atomic absorption/emission spectroscopy, electrochemical analysis, spectrophotometric analysis, liquid chromatography, and adsorptive stripping voltammetry.<sup>3–9</sup> These analytical approaches, however, require complex equipment, high operating costs, tedious preparation and time-consuming procedures. Thus, it is urgent to select an economical and effective analytical method for metal ion detection in aqueous solution.

CDs have been intensively studied since they were discovered occasionally in 2004.<sup>10</sup> Relative to traditional quantum dots and organic dyes,<sup>11</sup> CDs usually exhibit high fluorescence intensity, non-toxicity, excellent water solubility, chemical resistance, outstanding electronic properties and excellent biocompatibility.<sup>12–15</sup> These unique properties have enabled CDs to be widely applied in promising fields of sensors, metal ions detection, bio-imaging, drug delivery and light emitting diodes.<sup>16–22</sup> Among of them, the applications of CDs as fluorescence sensors for detecting and monitoring of metal ions have been studied. Furthermore, fluorescence quenching-recovery analysis has already been confirmed as the promising methods for metal ions detection due to its favorable

<sup>a</sup>Guangxi Key Laboratory of Clean Pulp & Papermaking and Pollution Control, School of Light Industry and Food Engineering, Guangxi University, Nanning, 530004, China. E-mail: wangzhiwei@gxu.edu.cn

<sup>b</sup>State Key Laboratory of Pulp and Paper Engineering, South China University of Technology, Guangzhou, 510641, China

<sup>c</sup>Liaoning Key Laboratory of Pulp and Paper Engineering, Dalian Polytechnic University, Dalian, 116034, China. E-mail: lihm@dlpu.edu.cn; guoyz@dlpu.edu.cn; Tel: +86-15164033963

<sup>d</sup>Shandong Huatai Paper Co., Ltd., Dongying, 275335, China

† Electronic supplementary information (ESI) available. See DOI: 10.1039/d1ra04972k



advantages, such as stable fluorescence, good selectivity, convenient and quick response.<sup>23,24</sup>

Owing to instant fluorescence response and excellent chemical activity, CDs-based fluorescence sensors, derived from various precursors, have been becoming more useful in selective and sensitive sensing platforms. Wang *et al.*<sup>25</sup> demonstrated that the photoexcited CDs can photoreduce the  $\text{Ag}^+$  to Ag in aqueous solution, suggesting that the photoexcited CDs were excellent electron donors as well as electron acceptors. Other literatures reported some common metal ions, such as  $\text{Fe}^{3+}$ ,<sup>26,27</sup>  $\text{Hg}^{2+}$ ,<sup>28</sup>  $\text{Cu}^{2+}$ ,<sup>29</sup>  $\text{As}^{3+}$ ,<sup>30</sup>  $\text{Pb}^{2+}$ ,<sup>31,32</sup>  $\text{Zn}^{2+}$ ,<sup>33</sup>  $\text{Au}^{3+}$ ,<sup>34</sup> could also selectively quench the fluorescence of CDs in the certain sensing systems. However, the sensitivity improvements for the CDs fluorescence quenching sense have been merely applied in one metal ion, which greatly limit their detection capability. Meanwhile, it was found that the detailed discussion on the fluorescence quenching mechanism of CDs had seldom been explored. Particularly, developing the deep explanations on the high-valence metal ions, which can result to obvious fluorescence quenching response of CDs compared with low-valence metal ions. There is a challenge to explore the phenomenon between different fluorescence quenching behaviors of CDs to diverse target metal ions. Consequently, the first aim of this work is that establishing the detailed fluorescence quenching mechanism between N-CDs and high-valence metal ions, because there still lacks detailed discussion on the quenching mechanism related to the high valence-state of metal ions and carbon dots in the current study. Secondly, it is practical significance to develop a multifunctional fluorescence sensing platform that satisfies simple operation, high sensitivity, and for high-valence metal ions detection in complex environment.

In this paper, we build a green approach for preparation N-CDs based on hydrothermal treatment of water-soluble CMC with EDA as exterior nitrogen-doping passivator. N-CDs with excellent blue fluorescence were obtained and possessed water dispersibility, good photostability, and a low level of cytotoxicity. The N-CDs aqueous solution served as the green fluorescence sensing probe to monitor the high-valence metal ions ( $\text{Fe}^{3+}$ ,  $\text{Cr}^{6+}$  and  $\text{Mn}^{7+}$ ) by fluorescence quenching response. Meanwhile, we further explored the quenching phenomenon of N-CDs to explain valence state-related electron-transfer between N-CDs and high-valence metal ions. Interestingly, the valence state-related fluorescence quenching phenomenon of N-CDs aqueous solution could be effectively recovered by introducing reducing agent ( $\text{Ti}^{3+}$ ). In addition, using the selectively fluorescence quenching behavior to  $\text{Fe}^{3+}$  as an example, the N-CDs were investigated on cellular imaging. These fluorescence recovery systems of N-CDs possessed fluorescence analytic prospect for high-valence metal ions sensing and biomedical.

## 2. Experimental

### 2.1 Materials

Carboxymethylcellulose (CMC, M. W. 90 000, 250 000, 700 000  $\text{g mol}^{-1}$ ), 1,2-propanediamine and 1,6-hexamethylenediamine were procured from Aladdin Chemistry Co., Ltd. Ethylenediamine (EDA, 99% purity) was purchased from Kermel Analytical

Reagent Co., Ltd.  $\text{CrCl}_3 \cdot 6\text{H}_2\text{O}$ ,  $\text{MgCl}_2$ ,  $\text{AgNO}_3$ ,  $\text{KCl}$ ,  $\text{MnCl}_2 \cdot 4\text{H}_2\text{O}$ ,  $\text{NaCl}$ ,  $\text{ZnCl}_2$ ,  $\text{BaCl}_2 \cdot 2\text{H}_2\text{O}$ ,  $\text{AlCl}_3$ ,  $\text{FeCl}_3 \cdot 6\text{H}_2\text{O}$ ,  $\text{CuCl}_2 \cdot 2\text{H}_2\text{O}$ ,  $\text{CaCl}_2$ ,  $\text{FeCl}_2 \cdot 4\text{H}_2\text{O}$  were obtained from Sinopharm Chemical Reagent Co., Ltd.  $\text{K}_2\text{CrO}_4$ ,  $\text{K}_2\text{Cr}_2\text{O}_7$ ,  $\text{KMnO}_4$ ,  $\text{TiCl}_3$ , glutathione (GSH), ascorbic acid,  $\text{SnCl}_4$  and hydroxylamine hydrochloride were supplied by Macklin Biochemical Co., Ltd.

### 2.2 Preparation of N-CDs

Typically, 2 g CMC (M. W. 90 000  $\text{g mol}^{-1}$ ) was dissolving in water (50 mL) with magnetic stirring. After that, 1.5 g EDA (or 1,2-propanediamine, 1,6-hexamethylenediamine) was slowly injected into the solution. Then, the mixture was then sealed into the stainless steel autoclave (100 mL) lined with Teflon and placed in an environment at 220 °C for 36 h of continuous heating. After that, the obtained solution was ultrasonically dispersed at 75 W for 30 min and then filtered by a filter membrane (0.22  $\mu\text{m}$ ). Finally, the solution was dialyzed in ultrapure water with a MWCO 500 Da dialysis membrane for 24 h. The powders of pure N-CDs were prepared by freeze-dried for 72 h. The other N-CDs were prepared using CMC (M. W. 250 000 and 700 000  $\text{g mol}^{-1}$ ) as the carbon source, and EDA as nitrogen dopant by the same hydrothermal treatment.

The sample obtained without the addition of EDA was designated CDs. 2 g CMC (M. W. 90 000  $\text{g mol}^{-1}$ ) was dissolving in 50 mL ultrapure water under vigorous magnetic stirring, and no EDA was added. Subsequent steps were similar to above mentioned procedures for preparing N-CDs.

### 2.3 Characterization

The morphology and size of sample were captured by a JEM-2100 microscope (Japan) at 200 kV. The functional groups of samples were achieved using Fourier I spectrophotometer (PerkinElmer, America) with frequencies ranging from 400 to 4000  $\text{cm}^{-1}$ . X-ray diffraction (XRD) patterns were obtained by a 6100 X-ray diffractometer (Shimadzu, Japan). The Raman analysis was investigated using a LabRAM ARAMIS Raman spectroscope (France) under excitation at 1064 nm. X-ray photoelectron spectroscopy (XPS) experiments were using an ESCALAB250Xi spectrometer (America).  $^{13}\text{C}$  NMR spectroscopy was acquired on a Bruker Avance 400 MHz spectrometer by dissolving 60 mg of N-CDs in 0.5 mL of deuterized water. All fluorescence measurements were performed at the Hitachi F-7000 fluorescence spectrophotometer (Japan).

### 2.4 Fluorescence quenching response

Initially, the 0.02  $\text{mg mL}^{-1}$  of N-CDs was used as stock solution. Different metal ions solutions ( $\text{Mg}^{2+}$ ,  $\text{K}^+$ ,  $\text{Na}^+$ ,  $\text{Ba}^{2+}$ ,  $\text{Fe}^{3+}$ ,  $\text{Ca}^{2+}$ ,  $\text{Al}^{3+}$ ,  $\text{Zn}^{2+}$ ,  $\text{Mn}^{2+}$ ,  $\text{Ag}^+$ ,  $\text{Cr}^{3+}$ ,  $\text{Cu}^{2+}$ ,  $\text{Fe}^{2+}$ ,  $\text{CrO}_4^{2-}$ ,  $\text{Cr}_2\text{O}_7^{2-}$  and  $\text{MnO}_4^-$ , 1000  $\mu\text{M}$ ), were mixed thoroughly with the stock solution. After equilibration for 5 min, all the fluorescence emissions were determined using a 360 nm excitation wavelength. The fluorescence intensity of N-CDs solution with and without metal ions was defined as  $F$  and  $F_0$ , respectively.

As a further investigation of the fluorescence sensitivity to high-valence state metal ions, 2 mL  $\text{Fe}^{3+}$ ,  $\text{CrO}_4^{2-}$ ,  $\text{Cr}_2\text{O}_7^{2-}$  and  $\text{MnO}_4^-$  ions aqueous solutions with various concentrations



were mixed with 2 mL N-CDs solution to form the fluorescence “turn off” sensing system. The fluorescence emission was performed after incubation for 5 min. The LOD was calculated as follows.

$$\text{LOD} = 3\sigma/K$$

where  $\sigma$  refers to the standard deviation of the blank ( $n = 11$ ),  $K$  refers to the slope for the range of the linearity.

## 2.5 Fluorescence recovering detection of reductants

The “turn off-on” fluorescence recovery system was constructed by introducing reductants. Briefly, various types of reductants with a final concentration of 1000  $\mu\text{M}$ , including  $\text{TiCl}_3$ , GSH, ascorbic acid,  $\text{SnCl}_4$  and hydroxylamine hydrochloride, were added into the above fluorescence “turn off” sensing system. After equilibration for 10 min, all emissions were measured by 360 nm excitation wavelengths. The fluorescence intensity of “turn off” sensing system was defined as  $F_{\text{F}}$ , while the fluorescence intensity of “turn off-on” sensing system was defined as  $F_{\text{R}}$ . The linear relationship was measured by introducing reductants with different concentrations.

## 2.6 Detecting high-valence metal ions in practical samples

To further study the practical application of the N-CDs for detecting high-valence metal ions under environmental wastewater simulated conditions, the standard addition method was carried out using river or lake water.<sup>35</sup> The tap water (TW) and lake water (LW) from school were filtered through a filter membrane (0.22  $\mu\text{m}$ ) to remove insoluble contaminants. 0.02  $\text{mg mL}^{-1}$  of N-CDs was used as stock solution, and different concentrations of  $\text{Fe}^{3+}$ ,  $\text{Cr}^{6+}$ , and  $\text{Mn}^{7+}$  ions aqueous solution were prepared using tap water and lake water, respectively. Analysis of the practical samples was performed using standard recovery method, and the specific experiment was as same as the modeling water.

## 2.7 Cytotoxicity evaluation and *in vitro* cellular imaging

The CCK-8 assay was to assess the cell viability of Vero cells. Briefly, Vero cells in 100  $\mu\text{L}$  DMEM solutions were incubated with 5%  $\text{CO}_2$  environment (37  $^{\circ}\text{C}$ , 24 h) in the 96-well plate. Vero cells were treated by the as-prepared N-CDs with 0–200  $\mu\text{g mL}^{-1}$  concentrations for one day or two days. 100  $\mu\text{L}$  of CCK-8 solutions were added and then cultured for 4 h. Thereafter, 150  $\mu\text{L}$  DMSO was replaced the medium comprising CCK-8 to adding the well. Finally, the optical density was captured by excited at 450 nm. The cytotoxicity evaluation and *in vitro* cellular imaging were presented in detail by previous paper.<sup>36</sup>

# 3. Results and discussion

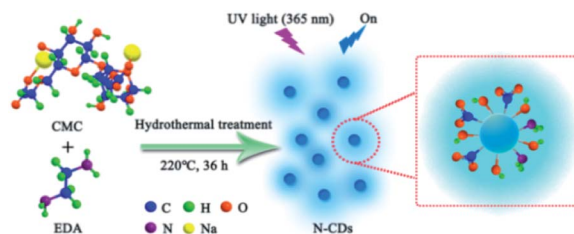
## 3.1 Preparation of fluorescence N-CDs

The fluorescence N-CDs were successfully obtained by mixing CMC and EDA through the green hydrothermal approach (220  $^{\circ}\text{C}$ , 36 h) (Scheme 1). Passivation of N-CDs with nitrogen was highly effective, which could endow obtained N-CDs with

high QY and stable fluorescence property. Aqueous solutions of N-CDs exhibited blue fluorescence under UV light (365 nm). The amino group was doped into the structure of N-CDs and played a key effect on the QY.<sup>36,37</sup> The effects of mass ratios of CMC to EDA, reaction temperature, molecular weights of CMC (M. W. 90 000, 250 000, 700 000  $\text{g mol}^{-1}$ ) and types of amine reagents on the QY values of N-CDs were further studied (Table S1†). The QY value of N-CDs was decreased from 22.9% to 15.4% and 14.7% with increasing the molecular weights of CMC from 90 000 to 250 000 and 700 000  $\text{g mol}^{-1}$ . The results confirmed that the CMC with higher molecular weights was not beneficial to enhancing the QY values of N-CDs. The N-CDs with blue fluorescence were also successfully prepared using different types of diamines (1,2-propanediamine and 1,6-hexamethylenediamine) as nitrogen dopant, and CMC (W. M. 90 000  $\text{g mol}^{-1}$ ) as the carbon source. However, the N-CDs possessed lower QY values (10.9% for 1,2-propanediamine and 13.4% for 1,6-hexamethylenediamine) than that of N-CDs using EDA as nitrogen dopant (22.9%). This result suggested that EDA as nitrogen dopant was more favorable to prepare the N-CDs with higher QY value. The QY value of non-nitrogen doped CDs was only 4.9%, suggesting that the nitrogen-doping treatment was beneficial to improve the QY value of N-CDs. Therefore, the optimal conditions were with 1 : 0.75 the mass ratio of CMC (M. W. 90 000  $\text{g mol}^{-1}$ ) to EDA for 36 h at 220  $^{\circ}\text{C}$ , and the QY value of N-CDs was reached 22.9%.

## 3.2 Structures of fluorescent N-CDs

The morphology and size distribution of the obtained N-CDs from CMC with different molecular weights were investigated by the TEM technique. The TEM images (Fig. 1a and b) of N-CDs obtained from CMC with M. W. 90 000  $\text{g mol}^{-1}$  showed the existence of well monodispersed spherical shapes with sizes in the range of 1–4 nm and a size of 2.3 nm, which was similar to that reported in related reports.<sup>38</sup> Furthermore, the size distribution of N-CDs, obtained from CMC with higher molecular weights (M. W. 250 000 and 700 000  $\text{g mol}^{-1}$ ), was also analysed by TEM technique (Fig. S1†). With increasing the molecular weight of CMC from 250 000 to 700 000  $\text{g mol}^{-1}$ , the average particle size of obtained N-CDs was increased to 6.3 and 7.0 nm, respectively. It could be caused by that CMC with higher molecular weight was incompletely reacted during the hydrothermal treatment process. The morphology of the obtained N-CDs still possessed spherical shape with good dispersability. The elemental compositions and structures of the obtained N-



Scheme 1 The synthetic diagram of fluorescent N-CDs.





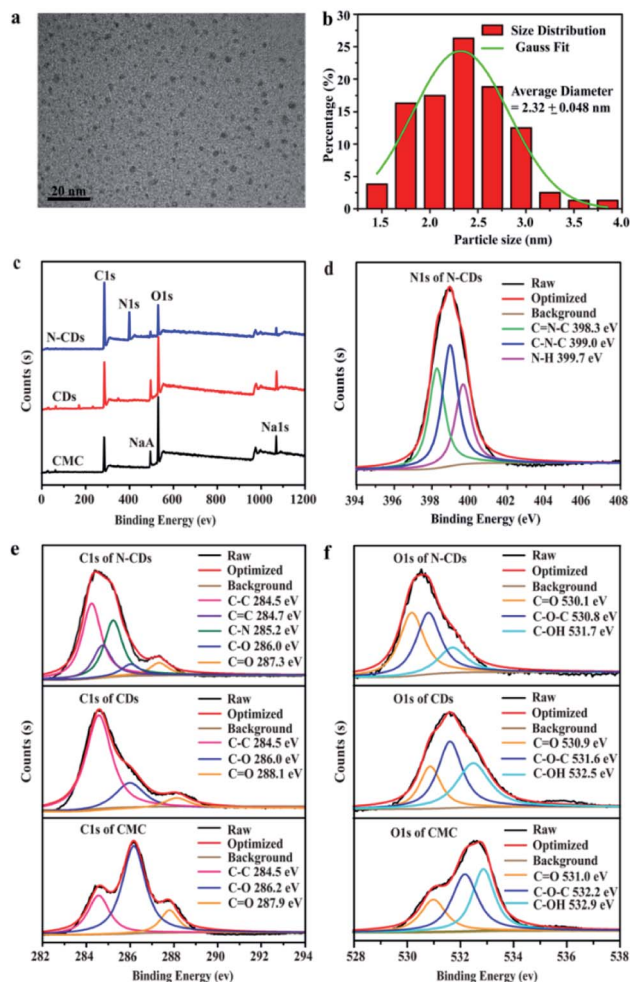


Fig. 1 TEM image (a) and particle size distribution (b) of N-CDs, XPS survey of CMC, CDs and N-CDs (c), N 1s of N-CDs (d), C 1s (e) and O 1s (f) of CMC, CDs and N-CDs.

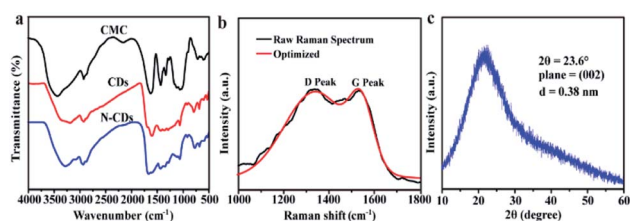


Fig. 2 FTIR spectra of CMC, CDs and N-CDs (a), Raman spectra (b) and XRD pattern (c) of N-CDs.

CDs were performed. In Fig. 1c, the peaks of C 1s, Na 1s, O 1s and Na 1s of CMC and CDs were observed at 285.6 eV, 496.6 eV, 532.6 eV and 1071.6 eV. The N-CDs displayed a new peak at 398.6 eV, relating to N 1s, revealing that nitrogen was introduced into the N-CDs. The carbon-to-oxygen ratio of samples increased as follows: CMC (1.44) < CDs (2.09) < N-CDs (5.78) (Table S2†). The main elemental compositions of N-CDs were C (68.75%), N (19.35%), and O (11.90%). The relative content of C-O and C=O bonds in CMC and CDs samples were very

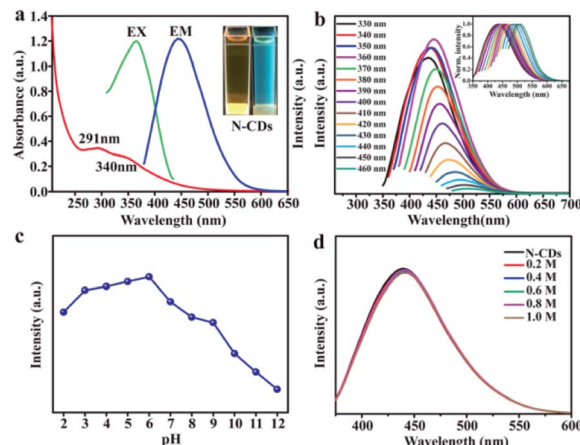


Fig. 3 UV-vis and the optimum excitation and emission fluorescence spectra of N-CDs (a), fluorescent properties of N-CDs with various excitation wavelengths (b), different pH (c) and concentrations of sodium chloride (d).

similar, which were 28.3% (C-O), 20.1% (C=O) in CMC and 27.5% (C-O), 20.1% (C=O) in CDs, respectively. However, the relative content of C-O (13.9%) and C=O (14.2%) bonds in N-CDs was significantly decreased, and the relative content of C-N bond was 24.2%. Therefore, the carboxyl and amino functional groups might be occurred dehydration and condensation reaction during the process of hydrothermal treatment. The nitrogen content of N-CDs was higher than those doping nitrogen content in reported literature.<sup>39</sup> A wide peak of nitrogen was observed in the range of 394 eV to 408 eV in the XPS spectra (Fig. 1d), which could be resolved into three distinct peaks around 398.3 eV, 399.0 eV and 399.7 eV, corresponding to the functional groups of C=N-C, C-N-C and N-H, respectively. Compared to CMC and CDs, the C 1s signals of N-CDs (Fig. 1e) were possessed a new C-N (285.2 eV) peak. The C=O and C-O peaks confirmed that N-CDs were rich in carboxyl and carbonyl functional groups. The O 1s signals (Fig. 1f) could be deconvoluted into three peaks at 531.0/530.9/530.1 eV (C=O), 532.2/531.6/530.8 eV (C-O-C) and 532.9/532.5/531.7 eV (C-OH), respectively.

FT-IR spectra were demonstrated in Fig. 2a. The extensive absorption of N-CDs at  $3279\text{ cm}^{-1}$  corresponds to the stretching vibration of O-H and N-H.<sup>35,40</sup> The existence of amino-containing groups in the N-CDs suggested that the nitrogen element was incorporated into N-CDs during the hydrothermal process. The peaks at  $1434\text{ cm}^{-1}$  and  $770\text{ cm}^{-1}$  in N-CDs indicated the presence of OH and C-O stretching vibration, respectively. Besides, C=O/C-N ( $1664\text{ cm}^{-1}$ ), C-O-C ( $1063\text{ cm}^{-1}$ ) and -COOH ( $917\text{ cm}^{-1}$ ) bonds were presented in the spectrum of N-CDs, confirming the presence of hydrophilic groups in the N-CDs.<sup>41</sup> Some oxygen-containing functional groups, such as O-H, C=O, and C-O groups, can improve the dispersibility and stability of N-CDs.<sup>42</sup> These results further validated the dehydration and condensation reactions of amino and carboxyl functional groups during high temperature heat treatment.

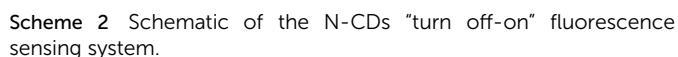
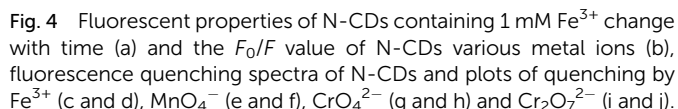


Figure 1 consists of four panels (a, b, c, d) showing XPS spectra. Each panel plots Counts (s) on the y-axis against Binding Energy (eV) on the x-axis. The spectra are deconvoluted into individual peaks and a background.

- Panel (a):** Fe 2p<sub>3/2</sub> spectrum. The x-axis ranges from 700 to 740 eV. The y-axis ranges from 0 to 10000 counts. Peaks are labeled at 711.2, 710.2, and 708.7 eV. The legend includes Raw (black), Optimized (red), Background (blue), Fe 2p<sub>3/2</sub> (green), and Fe 2p<sub>1/2</sub> (purple).
- Panel (b):** Fe 2p<sub>1/2</sub> spectrum. The x-axis ranges from 700 to 740 eV. The y-axis ranges from 0 to 10000 counts. Peaks are labeled at 710.2, 709.2, and 707.2 eV. The legend includes Raw (black), Optimized (red), Background (blue), Fe 2p<sub>3/2</sub> (green), Fe 2p<sub>1/2</sub> (purple), and Satellite (blue).
- Panel (c):** Ti 2p<sub>3/2</sub> spectrum. The x-axis ranges from 700 to 740 eV. The y-axis ranges from 0 to 10000 counts. Peaks are labeled at 710.2, 709.2, and 707.2 eV. The legend includes Raw (black), Optimized (red), Background (blue), Fe 2p<sub>3/2</sub> (green), Fe 2p<sub>1/2</sub> (purple), Satellite (blue), and Ti 2p<sub>3/2</sub> (green).
- Panel (d):** Ti 2p<sub>1/2</sub> spectrum. The x-axis ranges from 450 to 470 eV. The y-axis ranges from 0 to 10000 counts. Peaks are labeled at 458.7, 457.7, and 456.7 eV. The legend includes Raw (black), Optimized (red), Background (blue), Ti 2p<sub>3/2</sub> (green), and Ti 2p<sub>1/2</sub> (purple).

**Fig. 5** XPS spectra of N-CDs interacted with (a)  $\text{Fe}^{3+}$ , (b)  $\text{Fe}^{2+}$ , (c and e)  $\text{Fe}^{3+}$  and  $\text{Ti}^{3+}$ , (d)  $\text{Ti}^{3+}$ .

ascribed to the vibration of ordered  $\text{sp}^2$  hybridized carbon.<sup>43</sup> The intensity ratio of  $I_{\text{D}}/I_{\text{G}}$  value was 1.02, confirming the presence of abundant graphitic structures of N-CDs. XRD pattern (Fig. 2c) showed one peak at about  $23.6^\circ$ , which was similar to the (002) plane of graphite with disordered hybridization carbon. The interlayer spacing of N-CDs was 0.38 nm, higher than the graphite structure (0.34 nm), showing that the N-CDs possessed poor crystallization.  $^{13}\text{C}$  NMR spectroscopy was further exploited to gain chemical structure of the N-CDs (Fig. S2<sup>†</sup>). A series of peaks appeared in the range of 8–85 ppm, which was ascribed to  $\text{sp}^3$  carbons within the N-CDs.<sup>44</sup> The peaks between 100–170 ppm were attributed to  $\text{sp}^2$  carbons, and the peaks 170–185 ppm probably arose from carbonyl or carboxylic carbons in the N-CDs.<sup>45</sup> The results indicated that the carbon within the N-CDs was mainly with the type of  $\text{sp}^3$  structure, furthermore, small contents of  $\text{sp}^2$  carbons and carbonyl or carboxylic carbons were also present in the N-CDs.

The optical performances were investigated using UV-vis absorption, excitation and emission fluorescence techniques. The as-prepared N-CDs aqueous solution appeared light brown under daylight and displayed strong blue fluorescence by exposure under 365 nm UV lamp (Fig. 3a top-right inset). The aqueous solution of the N-CDs presented the absorption bands at 291 nm and 310 nm, which are ascribed to the  $\pi$ - $\pi^*$  transition of C=C and  $n$ - $\pi^*$  transition of C=O, respectively.<sup>46</sup> Furthermore, the optimum excitation was observed at 360 nm,

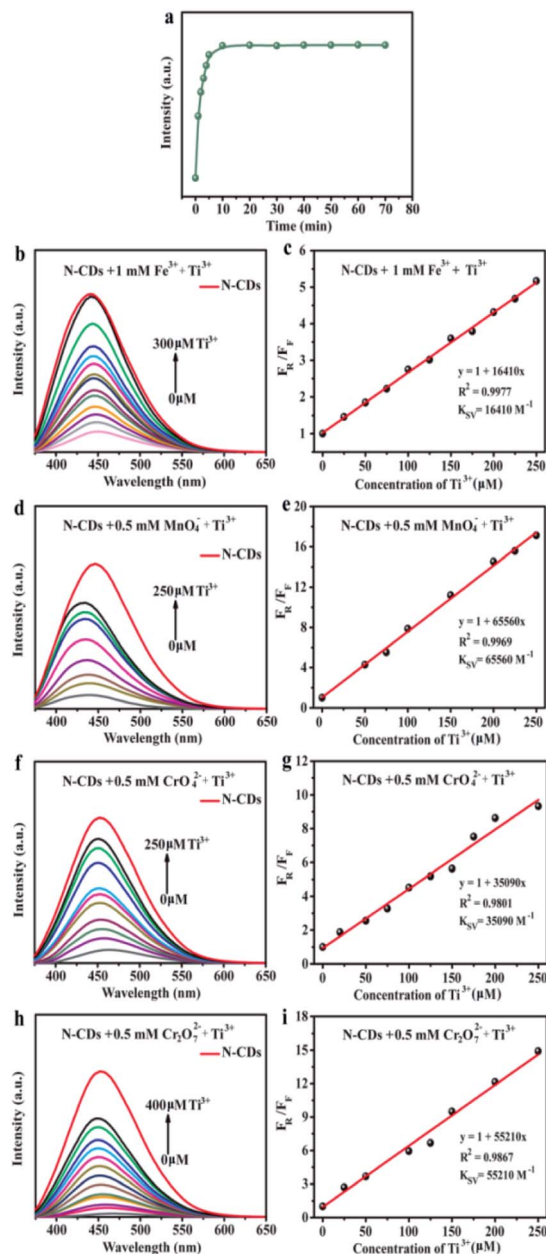


Fig. 6 Fluorescent recovery time of N-CDs/ $\text{Fe}^{3+}$  (1 mM) with  $\text{Ti}^{3+}$  (1 mM) (a), fluorescent recovery spectra and the plots of quenching of N-CDs/ $\text{Fe}^{3+}$  (b and c),  $\text{MnO}_4^-$  (d and e),  $\text{CrO}_4^{2-}$  (f and g) and  $\text{Cr}_2\text{O}_7^{2-}$  (h and i) systems with various concentrations  $\text{Ti}^{3+}$ .

while the emission wavelength was observed at 445 nm. In a similar way, the N-CDs exhibited excitation-dependent fluorescent behavior. When the excitation peak was changed with 330 nm to 460 nm, the corresponding fluorescence emission peak was red-shifted from 434 nm to 510 nm (Fig. 3b). This phenomenon was assigned to the state defect and particle distribution effect.

The impact of pH variation on the fluorescent properties was studied. In Fig. 3c, the N-CDs solution possessed excellent fluorescent stability in a weak acid environment ( $\text{pH} = 4-6$ ). In addition, the effects of ionic concentrations on fluorescent

properties of as-prepared N-CDs were further studied (Fig. 3d). The fluorescence intensity had no noticeable change with the concentration of sodium chloride solution increasing in the range from 0.2 M to 1.0 M. The results confirmed that the obtained N-CDs exhibited well fluorescent performance in high ionic concentration environments. The derived N-CDs were suitable to monitor metal ions owing to these fluorescence properties.

### 3.4 Fluorescent “turn off” sensing of high-valence state metal ions

To achieve the maximum fluorescent sensitivity, the equilibrium time was analysed. The fluorescent intensity of N-CDs sharply decreased within 5 min containing  $\text{Fe}^{3+}$  ions (1 mM), and then remained stable. Therefore, we selected 5 min as the incubation time in the detecting metal ions experiments. The relative fluorescent intensities towards various metal ions in aqueous solution were studied by excited at 360 nm (Fig. 4b). It was found that  $\text{Fe}^{3+}$  had a more pronounced quenching response to the fluorescence of N-CDs and the corresponding intensity decreased by 71.4% in the process, while the  $\text{Fe}^{2+}$  exhibited no significant difference. Compared with  $\text{Cr}^{3+}$  and  $\text{Mn}^{2+}$ , some types of high-valence metal ions, including  $\text{CrO}_4^{2-}$ ,  $\text{Cr}_2\text{O}_7^{2-}$  and  $\text{MnO}_4^-$ , could easily quench the fluorescence, which were 97.3%, 98.2% and 98.9%, respectively. Remarkably, the fluorescence behavior was evidently influenced only by those high-valence metal ions, but unchanged by the low-valence metal ions.

Fig. 4c was the fluorescence spectra of N-CDs containing various concentrations  $\text{Fe}^{3+}$ . The fluorescent intensity reduced till completely quenched when  $\text{Fe}^{3+}$  ions concentration was up to 1 mM. Furthermore, the Stern–Volmer curve revealed a well linearity ( $R^2 = 0.995$ ) (Fig. 4d). The Stern–Volmer constant ( $K_{\text{SV}}$ ) was  $4550 \text{ M}^{-1}$ , suggesting that N-CDs could be served as sensing platform to detect  $\text{Fe}^{3+}$  ions. The LOD value of  $\text{Fe}^{3+}$  ion was  $0.8 \mu\text{M}$ . Compared with other reported carbon dots from various precursors (Table S3†), the obtained N-CDs possessed wider linear range (0–1000  $\mu\text{M}$ ), and relatively low LOD ( $0.8 \mu\text{M}$ ) of  $\text{Fe}^{3+}$  ions. The results suggested that the N-CDs exhibited a favorable detection performance. Furthermore, similar “turn off” fluorescent phenomena could be observed in some high-valence metal ions ( $\text{MnO}_4^-$ ,  $\text{CrO}_4^{2-}$  and  $\text{Cr}_2\text{O}_7^{2-}$ ). Hence, the N-CDs aqueous solution was also used as fluorescence probes to detect  $\text{MnO}_4^-$ ,  $\text{CrO}_4^{2-}$  and  $\text{Cr}_2\text{O}_7^{2-}$  metal ions via the fluorescence quenching response. By introducing the high-valence metal ions into the N-CDs aqueous solution, fluorescent intensity was gradually reduced with the increase of  $\text{MnO}_4^-$ ,  $\text{CrO}_4^{2-}$  and  $\text{Cr}_2\text{O}_7^{2-}$  ions concentrations, respectively (Fig. 4e, g and i). Moreover, the fluorescence emission peaks were red-shifted in presence of  $\text{MnO}_4^-$ ,  $\text{CrO}_4^{2-}$  and  $\text{Cr}_2\text{O}_7^{2-}$  ions. The fluorescence quenching fitting curves between  $F_0/F$  value and metal ions concentrations were established and the results are shown in Fig. 4f, h and j. There were excellent correlation coefficients ( $R^2 > 0.991$ ) between the fluorescence quenching efficiency and high-valence metal ions ( $\text{MnO}_4^-$ ,  $\text{CrO}_4^{2-}$  and  $\text{Cr}_2\text{O}_7^{2-}$ ) concentrations from 0 to 100  $\mu\text{M}$ . The  $K_{\text{SV}}$  value was





Table 1 Detection results of high-valence metal ions in actual samples

Samples	Metal ions supplemented ( $\mu\text{M}$ )	Metal ions measured ( $\mu\text{M}$ )	Recovery (%)
$\text{Fe}^{3+}$ (WT)	10	10.76	107.6
$\text{Fe}^{3+}$ (WT)	50	50.32	100.64
$\text{Fe}^{3+}$ (LW)	10	9.45	94.5
$\text{Fe}^{3+}$ (LW)	60	61.75	102.9
$\text{Cr}^{6+}$ (WT)	10	9.83	98.3
$\text{Cr}^{6+}$ (WT)	60	61.24	102.06
$\text{Cr}^{6+}$ (LW)	10	9.27	92.7
$\text{Cr}^{6+}$ (LW)	50	48.21	96.4
$\text{Mn}^{7+}$ (WT)	10	9.52	95.2
$\text{Mn}^{7+}$ (WT)	30	31.67	105.5
$\text{Mn}^{7+}$ (LW)	10	9.03	90.3
$\text{Mn}^{7+}$ (LW)	30	29.38	97.9

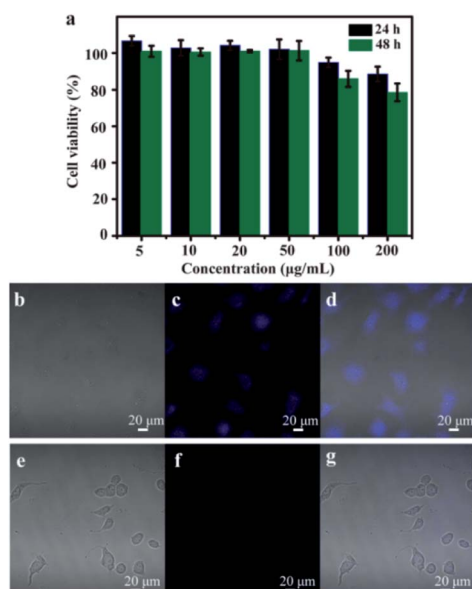


Fig. 7 The cell viability in various concentrations of N-CDs (a), microscopy photographs of N-CDs without/with  $\text{Fe}^{3+}$  (1 mM) under the bright field (b) and (e),  $\lambda_{\text{ex}} = 488 \text{ nm}$  (c) and (f), overlay (d) and (g), respectively.

calculated to be  $22\,160 \text{ M}^{-1}$  for  $\text{MnO}_4^-$ ,  $9620 \text{ M}^{-1}$  for  $\text{Cr}_2\text{O}_7^{2-}$  and  $5290 \text{ M}^{-1}$  for  $\text{CrO}_4^{2-}$ . These showed that N-CDs aqueous solution could be facily designed as sensitive and efficient detectors for high-valence metal ions, *e.g.*,  $\text{Fe}^{3+}$ ,  $\text{Mn}^{7+}$ ,  $\text{Cr}^{6+}$  ions, in the environmental pollution.

We discussed overlaps UV-vis spectra of different ions with fluorescent spectra of N-CDs (Fig. S3†). It was found that no new peak was occurred in the UV-vis spectra, showing that no new substance was formed. In addition, the overlaps area between UV-vis curve of  $\text{Fe}^{3+}$  and fluorescent emission curve of the N-CDs were small, confirming that fluorescence quenching by introducing  $\text{Fe}^{3+}$  to the N-CDs solution was thanks to the internal electron transfer, rather than fluorescence resonance energy transfer (FRET). For  $\text{CrO}_4^{2-}$ ,  $\text{Cr}_2\text{O}_7^{2-}$  and  $\text{MnO}_4^-$  metal ions, the large spectral overlaps areas of UV-vis curve and

fluorescent emission were corresponded to FRET, which could lay a foundation for detecting those mentioned metal ions by forming donor-acceptor (N-CDs-high valence metal ions) in different fluorescent systems. All of results indicated that the quenched fluorescence of N-CDs caused by metal ions was associated with their valence states.

### 3.5 Fluorescent “turn off-on” sensing of reducing agent

The valence of metal ions was reduced by introducing reducing agent, aiming to recover the quenched fluorescence of N-CDs aqueous solution. Therefore, the “turn off-on” fluorescence resuming system of N-CDs was constructed after adding reducing agents in the N-CDs/valence metal ions systems, which would broaden the application of N-CDs as fluorescence probe for reducing agent sensing. The  $F_{\text{R}}/F_{\text{F}}$  values, representing the fluorescent intensity ratio of the N-CDs solution containing valence metal ions (1 mM) without and with reducing agents (1 mM), are shown in Table S4.† The higher  $F_{\text{R}}/F_{\text{F}}$  value indicated that the fluorescence resuming efficiency was better by introducing reducing agents. Reducing agents, including  $\text{Ti}^{3+}$ , ascorbic acid,  $\text{Sn}^{4+}$ , hydroxylamine hydrochloride and GSH, were used to reversibly change the fluorescence. Among all of these reducing agents,  $\text{Ti}^{3+}$  had the best fluorescence resuming ability to the quenched fluorescence. In the case of  $\text{Ti}^{3+}$ -reduction fluorescence resuming of N-CDs, the maximal resuming rates were calculated to be 96.4% for  $\text{Fe}^{3+}$ , 58.8% for  $\text{MnO}_4^-$ , 87.4% for  $\text{CrO}_4^{2-}$  and 84.8% for  $\text{Cr}_2\text{O}_7^{2-}$ . The fluorescence recovery performance was attributed to the redoxability of reducing agent, suggesting that redox process between the surface groups of N-CDs and metal ions was the driving force to result in the fluorescence recovering.

Here we designed a schematic diagram to reveal the “turn off-on” fluorescence resuming system between N-CDs/valence metal ions and reducing reagents. A simple fluorescence system was established based on the aqueous solution of N-CDs with high-valence metal ions ( $\text{Fe}^{3+}$ ,  $\text{Mn}^{7+}$ ,  $\text{Cr}^{6+}$ ) as the fluorescence quencher. The obtained N-CDs solution showed blue light using UV lamp at 365 nm (Scheme 2). The blue fluorescence was disappeared (turn off) when  $\text{Fe}^{3+}$ ,  $\text{Mn}^{7+}$  and  $\text{Cr}^{6+}$  high-



valence metal ions were mixed with the N-CDs solution. Taking the  $\text{Fe}^{3+}$  metal ions as an example, specific information of the surface state of N-CDs after  $\text{Fe}^{3+}$ ,  $\text{Fe}^{2+}$  and  $\text{Fe}^{3+}\text{-Ti}^{3+}$  absorption was recorded by XPS spectra, which could be further studied the correlation between metal ions and surface groups of N-CDs (Fig. 5). The peaks of  $\text{Fe } 2p_{3/2}$  and  $\text{Fe } 2p_{1/2}$  in the presence of  $\text{Fe}^{3+}$  were observed at 711.2 eV and 724.0 eV, respectively (Fig. 5a). In the spectrum of  $\text{Fe}^{2+}$  sample (Fig. 5b), the peaks of  $\text{Fe } 2p_{3/2}$  and  $\text{Fe } 2p_{1/2}$  appeared at 710.2 eV and 723.8 eV, which possessed lower binding energy than that of  $\text{Fe}^{3+}$ /N-CDs.<sup>47</sup> This might be due to the strong electrostatic interaction between  $\pi$  electrons in the N-CDs and the empty orbital of  $\text{Fe}^{3+}$ , resulting in the quenching fluorescence. As shown in Fig. 5c, the signal peaks of  $\text{Fe } 2p_{3/2}$  and  $\text{Fe } 2p_{1/2}$  in N-CDs/ $\text{Fe}^{3+}/\text{Ti}^{3+}$  sample appeared at 710.2 eV and 723.8 eV, which was consistent with binding energy of  $\text{Fe}^{2+}$  in N-CDs/ $\text{Fe}^{2+}$  sample. The results indicated that  $\text{Fe}^{3+}$  was reduced to  $\text{Fe}^{2+}$  after introducing  $\text{Ti}^{3+}$  metal ions into the N-CDs/ $\text{Fe}^{3+}$  solution, and the quenched fluorescence could be restored owing to the redox process. Besides, the Ti metal ions of valence state and the peak position were further analysed to verify the above hypothesis by XPS spectra (Fig. 5d and e). In the XPS spectrum (Fig. 5d) of N-CDs solution only addition  $\text{Ti}^{3+}$ , two peaks of  $\text{Ti } 2p_{3/2}$  and  $\text{Ti } 2p_{1/2}$  were presented in 458 eV and 463.7 eV. However, after addition of  $\text{Ti}^{3+}$  metal ion into the N-CDs/ $\text{Fe}^{3+}$  solution (Fig. 5e), the peaks of  $\text{Ti } 2p_{3/2}$  and  $\text{Ti } 2p_{1/2}$  was shifted to high binding energy (458.7 eV, 464.6 eV), showing that electron transfer might occurred between  $\text{Ti}^{3+}$  metal ion and N-CDs/ $\text{Fe}^{3+}$  system by the redox process, which could reduce high-valence metal ions to low-valence metal ions for further realize the recovery of fluorescence.

Based on the above “turn off-on” fluorescence sensing system,  $\text{Ti}^{3+}$  could effectively lead to fluorescent resuming of the N-CDs quenched by high valence metal ions. Therefore, the impacts of the different concentrations  $\text{Ti}^{3+}$  on the fluorescent recovery performance of N-CDs/high valence metal ions systems were further investigated (Fig. 6). The fluorescent intensity of the N-CDs/ $\text{Fe}^{3+}$  system with  $\text{Ti}^{3+}$  peaked when incubation for 10 min (Fig. 6a). Therefore, we selected 10 min as the optimal equilibrium time to detect  $\text{Ti}^{3+}$ . Interestingly, “turn off-on” fluorescence recovery intensity was gradually increased when the  $\text{Ti}^{3+}$  was added into the N-CDs/valence metal ions systems. The fluorescence recovery emission curves showed blue-shift with increasing the  $\text{Ti}^{3+}$  contents (Fig. 6b, d, f and h). In addition, there was good linear relation ( $R^2 > 0.98$ ) between  $F_R/F_F$  and the concentration of  $\text{Ti}^{3+}$  (0–250  $\mu\text{M}$ ) (Fig. 6c, e, g and i). The  $K_{sv}$  of fluorescence recovery fitting curve after introducing  $\text{Ti}^{3+}$  was calculated to be 16 410  $\text{M}^{-1}$ , 65 560  $\text{M}^{-1}$ , 35 090  $\text{M}^{-1}$  and 55 210  $\text{M}^{-1}$  for the N-CDs/ $\text{Fe}^{3+}$ , N-CDs/ $\text{MnO}_4^-$ , N-CDs/ $\text{CrO}_4^{2-}$  and N-CDs/ $\text{Cr}_2\text{O}_7^{2-}$ , respectively. Hence, taking advantage of the novel “turn off-on” fluorescence system, the comprehensive approach for analysis  $\text{Ti}^{3+}$  was great promising in the application of daily wastewater and environment monitoring.

### 3.6 Analysis of the practical samples

To further evaluate the practical application of the as-prepared N-CDs for detecting metal ions in the actual samples, the

standard recovery experiments were performed using TW from laboratory and LW from school. The water samples were filtered through a filter membrane (0.22  $\mu\text{m}$ ). The different concentrations of  $\text{Fe}^{3+}$ ,  $\text{Cr}^{6+}$ , and  $\text{Mn}^{7+}$  were added into the N-CDs solution. Despite the rich minerals and impurities present in the lake water, there was no distinct effect on the detecting metal ions, as shown in Table 1. The standard recovery rate of  $\text{Fe}^{3+}$ ,  $\text{Cr}^{6+}$ , and  $\text{Mn}^{7+}$  with various concentrations was in the range of 94.5–107.6%, 92.7–102.06%, and 90.3–105.5%, respectively. The results indicated that the current method might provide an efficient path for detecting high-valence metal ions in actual samples.

### 3.7 Bio-imaging with N-CDs

As to be applied in the field of bio-imaging, the requirement for N-CDs is relatively low toxicity. Therefore, the bio-toxicity of as-prepared N-CDs in Vero cells was further investigated. Vero cells were incubated in DMEM at varying concentrations of N-CDs for one day or two days. The cell viability still remained 86% after incubated in DMEM with N-CDs (100  $\mu\text{g mL}^{-1}$ ) for two days (Fig. 7a). The results indicated that N-CDs were no cytotoxic, have good compatible with Vero cells as fluorescent probes for biosensors.<sup>48–50</sup> On account of the excellent fluorescent properties and superior biocompatibility, the N-CDs could be regarded as sensor in cellular imaging. After incubation for 4 h in N-CDs solution, intracellular blue-colored fluorescence was seen by 488 nm excitation wavelength (Fig. 7b–d), confirming that the obtained N-CDs solution was effectively internalized by Vero cells. However, no fluorescence appeared when Vero cells were mixed in N-CDs/ $\text{Fe}^{3+}$  (1 mM) solution (Fig. 7e–g). The N-CDs products from CMC and EDA can be employed as promising fluorescent sensor for cell image-forming and biomarker.

## 4. Conclusions

In summary, we demonstrated stable N-CDs with high levels of QY (22.9%) by a single-step hydrothermal method employing CMC and EDA as precursors. The corresponding N-CDs were spherical shape with 2.3 nm average diameter as well as excellent water dispersibility. The obtained N-CDs exhibited selective quenching response by a series of high-valence ( $\text{Fe}^{3+}$ ,  $\text{Cr}^{6+}$  and  $\text{Mn}^{7+}$ ) metal ions. By introducing  $\text{Fe}^{3+}$  ion as a model quencher, the LOD of  $\text{Fe}^{3+}$  ion was 0.8  $\mu\text{M}$ . We have further explored that the quenching mechanism of N-CDs by high valence metal ions to explain valence state-related electron-transfer fluorescence quenching between high-valence metal ions and N-CDs. An interesting finding was that the quenched fluorescence could be effectively recovered by reducing agent ( $\text{Ti}^{3+}$ ). Therefore, N-CDs were served as reversible fluorescent sensors for detecting reducing agent on the basis of the high-valence metal ions induced fluorescence quenching of the N-CDs. The sensing platform with high-efficiency and instant fluorescence response will give highlight on developing smart devices for monitoring high-valence metal ions and environmental redox substances in wastewater.





## Author contributions

Project was conceived by Yanzhu Guo and Zhenzhen Liu. Experiments were designed by Yanzhu Guo, Zhenzhen Liu and Runsen Li. Laboratory work by Zhenzhen Liu, Runsen Li and Yumei Gong. Data analysis was carried out by Yanzhu Guo, Zhenzhen Liu, Yan Li and Jingpeng Zhou. Manuscript was written by Zhenzhen Liu, Yanzhu Guo, Haiming Li and Hai-qiang Shi and edited by Zhenzhen Liu, Yanzhu Guo, Zhiwei Wang and Fengshan Zhang.

## Conflicts of interest

There are no conflicts to declare.

## Acknowledgements

We are grateful for the National Natural Science Foundation (22078036 and 31500493), Liaoning Revitalization Talents Program (XLYC1807232), Liaoning BaiQianWan Talents Program, the State Key Laboratory of Pulp and Paper Engineering, South China University of Technology (202002) and the Opening Project of Guangxi Key Laboratory of Clean Pulp & Papermaking and Pollution Control (2019KF30) for their support of this research.

## References

- 1 F. S. Al-Fartusie and S. N. Mohssan, *Indian J. Adv. Chem. Sci.*, 2017, **5**, 127.
- 2 J. Jiang, S. Y. Pang, J. Ma and H. Liu, *Environ. Sci. Technol.*, 2012, **46**, 1774.
- 3 S. G. Tuncel, S. Yenisoy-Karakas and A. Dogangun, *Talanta*, 2004, **63**, 273.
- 4 M. Ghaedi, K. Niknam, A. Shokrollahi, E. Niknam, H. R. Rajabi and M. Soylak, *J. Hazard. Mater.*, 2008, **155**, 121.
- 5 S. Khazaeli, N. Nezamabadi, M. Rabani and H. A. Panahi, *Microchem. J.*, 2013, **106**, 147.
- 6 G. Aragay and A. Merkoçi, *Electrochim. Acta*, 2012, **84**, 49.
- 7 K. Agrawal, K. S. Patel, K. Shrivastava, V. K. Jain and F. Khan, *J. Hazard. Mater.*, 2009, **164**, 95.
- 8 H. S. Amoli, A. Porgam, Z. B. Sadr and F. Mohanazadeh, *J. Chromatogr. A*, 2006, **1118**, 82.
- 9 P. Ugo, L. M. Moretto and G. A. Mazzocchin, *Anal. Chim. Acta*, 1995, **305**, 74.
- 10 X. Xu, R. Ray, Y. Gu, H. J. Ploehn, L. Gearheart, K. Raker and W. A. Scrivens, *J. Am. Chem. Soc.*, 2004, **126**, 12736.
- 11 G. Y. Lan, Y. W. Lin, Y. F. Huang and H. T. Chang, *J. Mater. Chem.*, 2007, **17**, 2661.
- 12 Q. Li, T. Ohulchanskyy, R. Liu, K. Koynov, D. Wu, A. Best and R. Kumar, *J. Phys. Chem. C*, 2010, **114**, 12062.
- 13 S. Y. Park, H. U. Lee, E. S. Park, S. C. Lee, J. W. Lee, S. W. Jeong, C. H. Kim, Y. C. Lee, Y. S. Huh and J. Lee, *ACS Appl. Mater. Interfaces*, 2014, **6**, 3365.
- 14 Y. W. Zheng, D. Yang, X. Wu, H. R. Yan, Y. C. Zhao, B. Feng, K. Duan, J. Weng and J. X. Wang, *RSC Adv.*, 2015, **5**, 90245.
- 15 B. De and N. Karak, *RSC Adv.*, 2013, **3**, 8286.
- 16 H. Huang, C. Li, S. Zhu, H. Wang, C. Chen, Z. Wang, T. Bai, Z. Shi and S. Feng, *Langmuir*, 2014, **30**, 13542.
- 17 X. Tan, A. N. B. Romainor, S. F. Chin and S. M. Ng, *J. Anal. Appl. Pyrolysis*, 2014, **105**, 157.
- 18 K. Hola, Y. Zhang, Y. Wang, E. P. Giannelis, R. Zboril and A. L. Rogach, *Nano Today*, 2014, **9**, 590.
- 19 F. Lu, Y. Song, H. Huang, Y. Liu, Y. Fu, J. Huang, H. Li, H. Qu and Z. Kang, *Carbon*, 2017, **120**, 95.
- 20 Y. Shu, J. Lu, Q. X. Mao, R. S. Song, X. Y. Wang, X. W. Chen and J. H. Wang, *Carbon*, 2017, **114**, 324.
- 21 L. H. Mao, W. Q. Tang, Z. Y. Deng, S. S. Liu, C. F. Wang and S. Chen, *Ind. Eng. Chem. Res.*, 2014, **53**, 6417.
- 22 P. J. G. Luo, F. Yang, S. T. Yang, S. K. Sonkar, L. J. Yang, J. J. Broglie, Y. Liu and Y. P. Sun, *RSC Adv.*, 2014, **4**, 10791.
- 23 W. Gao, H. Song, X. Wang, X. Liu, X. Pang, Y. Zhou, B. Gao and X. Peng, *ACS Appl. Mater. Interfaces*, 2018, **10**, 1147.
- 24 L. Rao, Y. Tang, H. Lu, S. Yu, X. Ding, K. Xu, Z. Li and J. Z. Zhang, *Nanomaterials*, 2018, **8**, 900.
- 25 X. Wang, L. Cao, F. Lu, M. J. Mezziani, H. Li, G. Qi, B. Zhou, B. A. Harruff, F. Kermarrec and Y. P. Sun, *Chem. Commun.*, 2009, **25**, 3774.
- 26 K. Qu, J. Wang, J. Ren and X. Qu, *Chem.-Eur. J.*, 2013, **19**, 7243.
- 27 T. N. J. I. Edison, R. Atchudan, J. J. Shim, S. Kalimuthu, B. C. Ahn and Y. R. Lee, *J. Photochem. Photobiol., B*, 2016, **158**, 235.
- 28 Y. Yan, H. Yu, K. Zhang, M. Sun, Y. Zhang, X. Wang and S. Wang, *Nano Res.*, 2016, **9**, 2088.
- 29 N. Gogoi, M. Barooah, G. Majumdar and D. Chowdhury, *ACS Appl. Mater. Interfaces*, 2015, **7**, 3058.
- 30 A. Saikia and N. Karak, *Mater. Today Commun.*, 2018, **14**, 82.
- 31 A. Kumar, A. R. Chowdhuri, D. Laha, T. K. Mahto, P. Karmakar and S. K. Sahu, *Sens. Actuators, B*, 2017, **242**, 679.
- 32 R. Bandi, R. Dadigala, B. R. Gangapuram and V. Guttena, *J. Photochem. Photobiol., B*, 2018, **178**, 330.
- 33 W. J. Niu, D. Shan, R. H. Zhu, S. Y. Deng, S. Cosnier and X. J. Zhang, *Carbon*, 2016, **96**, 1034.
- 34 V. Sharma, N. Kaur, P. Tiwari, A. K. Saini and S. M. Mobin, *Carbon*, 2018, **139**, 393.
- 35 Y. Liu, Y. Liu, S. J. Park, Y. Zhang, T. Kim, S. Chae, M. Park and H. Y. Kim, *J. Mater. Chem. A*, 2015, **3**, 17747.
- 36 Z. Z. Liu, M. J. Chen, Y. Z. Guo, J. H. Zhou, Q. S. Shi and R. C. Sun, *Chem. Eng. J.*, 2020, **384**, 123260.
- 37 B. Han, W. Wang, H. Wu, F. Fang, N. Wang, X. Zhang and S. Xu, *Colloids Surf., B*, 2012, **100**, 209.
- 38 Y. Li, J. Ren, R. Sun and X. Wang, *J. Biomed. Nanotechnol.*, 2018, **14**, 1543.
- 39 P. Shen, J. Gao, J. Cong, Z. Liu, C. Li and J. Yao, *ChemistrySelect*, 2016, **1**, 1314.
- 40 X. Yang, Y. Zhuo, S. Zhu, Y. Luo, Y. Feng and Y. Dou, *Biosens. Bioelectron.*, 2014, **60**, 292.
- 41 A. Gupta, N. C. Verma, S. Khan and C. K. Nandi, *Biosens. Bioelectron.*, 2016, **81**, 465.
- 42 S. Qu, X. Wang, Q. Lu, X. Liu and L. Wang, *Angew. Chem., Int. Ed.*, 2012, **51**, 12215.



- 43 D. Qu, M. Zheng, P. Du, Y. Zhou, L. Zhang, D. Li, H. Tan, Z. Zhao, Z. Xie and Z. Sun, *Nanoscale*, 2013, **5**, 12272.
- 44 K. J. D. MacKenzie and M. E. Smith, *Multinuclear solid-state NMR of inorganic materials*, Pergamon, Oxford, 2002.
- 45 L. Tian, D. Ghosh, W. Chen, S. Pradhan, X. Chang and S. Chen, *Chem. Mater.*, 2009, **21**, 2803.
- 46 H. Li, W. Kong, J. Liu, N. Liu, H. Huang, Y. Liu and Z. Kang, *Carbon*, 2015, **91**, 66.
- 47 Q. Mei, C. Jiang, G. Guan, K. Zhang, B. Liu, R. Liu and Z. Zhang, *Chem. Commun.*, 2012, **48**, 7468.
- 48 Z. Zhang, W. Sun and P. Wu, *ACS Sustainable Chem. Eng.*, 2015, **3**, 1412.
- 49 S. Zhu, Q. Meng, L. Wang, J. Zhang, Y. Song, H. Jin, K. Zhang, H. Sun, H. Wang and B. Yang, *Angew. Chem., Int. Ed.*, 2013, **52**, 3953.
- 50 X. Chen, Q. Jin, L. Wu, C. Tung and X. Tang, *Angew. Chem., Int. Ed.*, 2104, **3**, 542.

